JACS
JOURNAL OF THE AMERICAN CHEMICAL SOCIETY
Article
pubs.acs.org/JACS

Unraveling the Molecular Structures of Asphaltenes by Atomic Force Microscopy

Bruno Schuler,*[,†] Gerhard Meyer,[†] Diego Peña,[‡] Oliver C. Mullins,[§] and Leo Gross*[,†]

[†]IBM Research − Zurich, Säumerstrasse 4, 8803 Rüschlikon, Switzerland
[‡]CIQUS and Facultad de Química, Universidad de Santiago de Compostela, E-15782 Santiago de Compostela, Spain
[§]Schlumberger-Doll Research, Cambridge, Massachusetts 02139, United States

Supporting Information

ABSTRACT: Petroleum is one of the most precious and complex molecular mixtures existing. Because of its chemical complexity, the solid component of crude oil, the asphaltenes, poses an exceptional challenge for structure analysis, with tremendous economic relevance. Here, we combine atomic-resolution imaging using atomic force microscopy and molecular orbital imaging using scanning tunnelling microscopy to study more than 100 asphaltene molecules. The complexity and range of asphaltene polycyclic aromatic hydrocarbons are established in detail. Identifying molecular structures provides a foundation to understand all aspects of petroleum science from colloidal structure and interfacial interactions to petroleum thermodynamics, enabling a first-principles approach to optimize resource utilization. Particularly, the findings contribute to a long-standing debate about asphaltene molecular architecture. Our technique constitutes a paradigm shift for the analysis of complex molecular mixtures, with possible applications in molecular electronics, organic light emitting diodes, and photovoltaic devices.

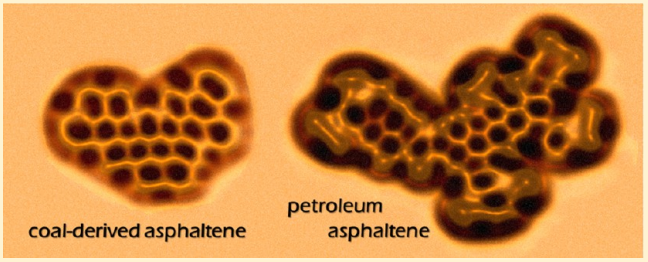

INTRODUCTION

In nature, molecules generally exist in mixtures. Petroleum is probably the most prominent of such mixtures and one of the most complex materials encountered with possibly over 100,000 distinct chemical constituents.[1,2] The primary unresolved component of crude oil is asphaltene.[2−4] Understanding the structure of asphaltenes is of immense economic importance[2,4−8] and a prerequisite to establishing the structure−function relationship in petroleomics,[2] but their molecular architecture has been subject to a long-standing debate.[3,9−13] Specifically, some studies indicate that individual asphaltene molecules contain primarily one polycyclic aromatic hydrocarbon (PAH)[3,12] ("island"), while other studies indicate that structures with multiple PAHs ("archipelago") contribute.[13] Difficulties associated with resolving this issue include formation of archipelago from island structures in experiments[14] and the potential inability to disaggregate asphaltene aggregates.[15] Recent experiments using laser desorption have established disaggregation of asphaltenes and have obtained dominance of island structures,[16] consistent with other mass spectral measurements.[17]

Asphaltenes are linked to many key economic issues in the petroleum industry today. Unwanted asphaltene phase transitions hinder petroleum production, transportation, and refining.[2,4] Asphaltene interfacial activity with rocks affects wettability, offering a focal point for enhanced oil recovery.[8] New asphaltene thermodynamics is used to evaluate the extent of fluid equilibrium in reservoirs, indicating flow connectivity, the most important reservoir uncertainty.[18] In addition, understanding the chemical processes that occur in oil reservoirs[6,7] is improved by accurate structural characterization. The capability to address all of these concerns is founded on an accurate representation of asphaltene molecules. However, the structure analysis of asphaltenes has posed an exceptional challenge because of their chemical complexity that is only now being resolved.[19]

Scanning probe microscopy offers the unique capability of imaging *single* adsorbates at the atomic scale. The characterization of asphaltenes had been attempted with scanning tunnelling microscopy (STM),[20,21] but to date no atomic-resolution could be achieved on asphaltene molecules. Recent progress in atomic force microscopy (AFM) enabled visualization of the atomic structure of individual molecules in real space.[22] This method was also used to analyze bond order,[23] identify the molecular structure of natural compounds[24,25] and graphene nanoribbons,[26] and detect products of chemical synthesis[27] and on-surface reactions.[28,29] By using STM and ultrathin insulating films as a substrate, one can also map molecular orbitals.[30−32]

Here, we present atomic-resolution low-temperature AFM data of individual molecules of asphaltene, one of the most complex and intriguing natural mixtures existing. Additionally, orbital imaging with the STM is used to access the polycyclic

Received: April 20, 2015
Published: July 14, 2015

DOI: 10.1021/jacs.5b04056
J. Am. Chem. Soc. 2015, 137, 9870−9876

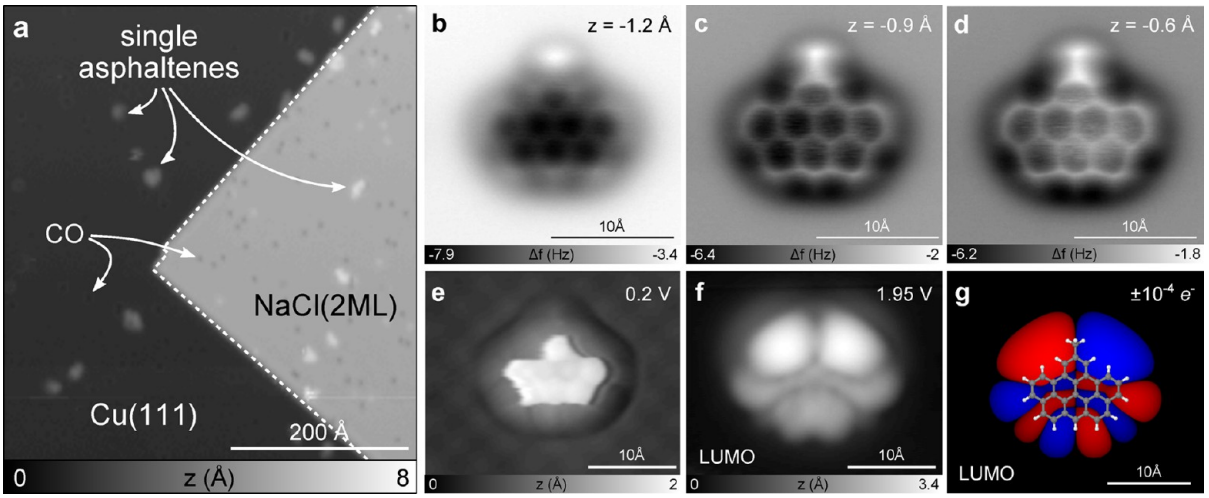

Figure 1. Coal-derived asphaltene sample preparation and **CA1**. (a) STM overview image (I = 1 pA, V = 0.5 V) of the CA sample on NaCl(2 ML)/Cu(111).(b–d) AFM images of **CA1** on NaCl(2 ML)/Cu(111) at different set-points z from (I = 1.4 pA, V = 0.2 V). (e) STM image of **CA1** (I = 10 pA, V = 0.2 V). (f) STM image at the NIR (I = 1.4 pA, V = 1.95 V). (g) LUMO orbital of **CA1** with the molecular structure overlaid as a guide to the eye. CO-functionalized tips have been used for all AFM and STM measurements shown.

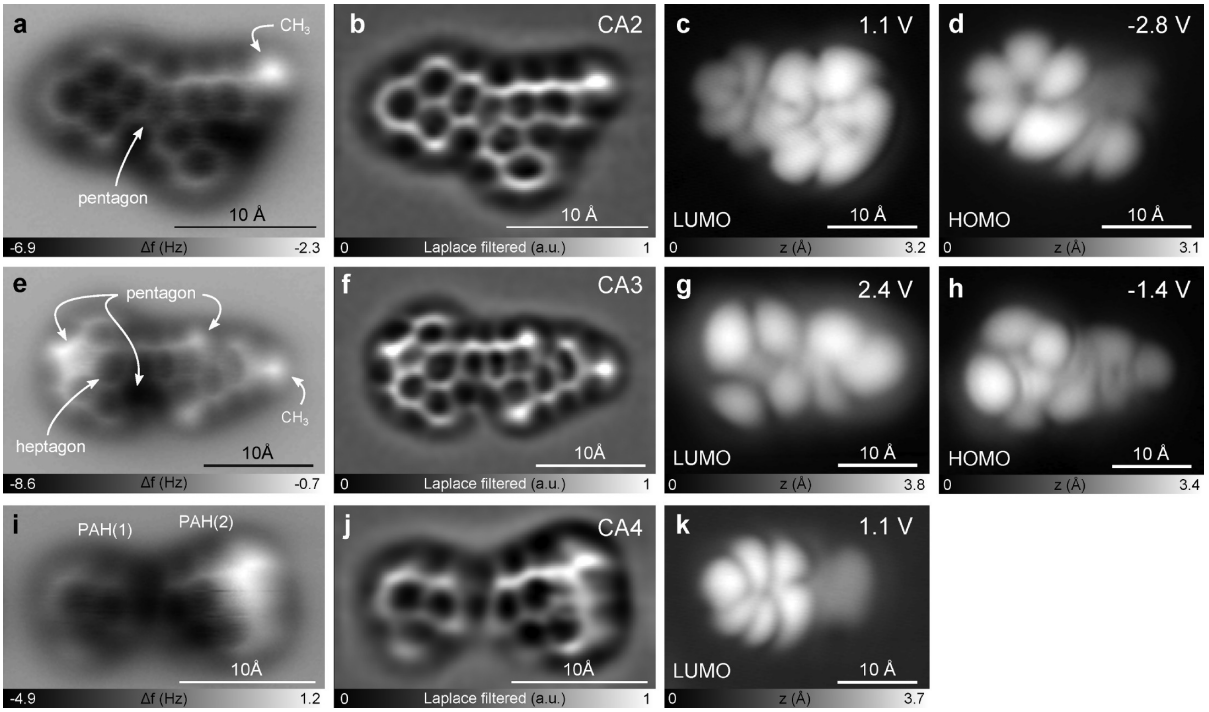

Figure 2. Coal-derived asphaltenes **CA2**–**CA4**. (a,b) AFM image of **CA2** on NaCl(2 ML)/Cu(111) (a) and the Laplace-filtered image (b). (c,d) STM orbital images (I = 1.4 pA) of **CA2** corresponding to the LUMO and HOMO resonance, respectively. (e,f) AFM image of **CA3** on NaCl(2 ML)/Cu(111) (e) and the Laplace-filtered image (f). (g,h) STM orbital images (I = 1.4 pA) of **CA3** corresponding to the LUMO and HOMO resonance, respectively. (i,j) AFM image of **CA4** on NaCl(2 ML)/Cu(111) (i) and the Laplace-filtered image (j). (k) STM orbital image of **CA4** corresponding to the LUMO resonance.

aromatic hydrocarbon (PAH) moieties of asphaltene, their primary site of intermolecular interaction. This combination of AFM and STM investigations of individual molecules demonstrates a methodology for structural assignment within mixtures with unprecedented resolution and moreover could be used as a powerful method to screen mixtures for novel molecules for molecular electronics[33,34] and applications in organic light emitting diodes and photovoltaic devices.[35]

As a substrate, a Cu(111) single crystal partially covered with islands of two-monolayer NaCl (denoted as NaCl(2 ML)/Cu(111)) was used. A small coverage (<5% ML) of individual asphaltene molecules was prepared by thermal evaporation by flash-heating from a silicon wafer onto the substrate at 10 K. We compare asphaltenes from different sources: (i) coal-derived asphaltenes (CAs) and (ii) petroleum asphaltenes (PAs). An STM overview image of the CA sample preparation is shown in Figure 1a. All STM and AFM measurements shown here were recorded in constant-current and constant-height modes, respectively, with a CO tip (see Materials and Methods section for details).

DOI: 10.1021/jacs.5b04056
J. Am. Chem. Soc. 2015, 137, 9870–9876

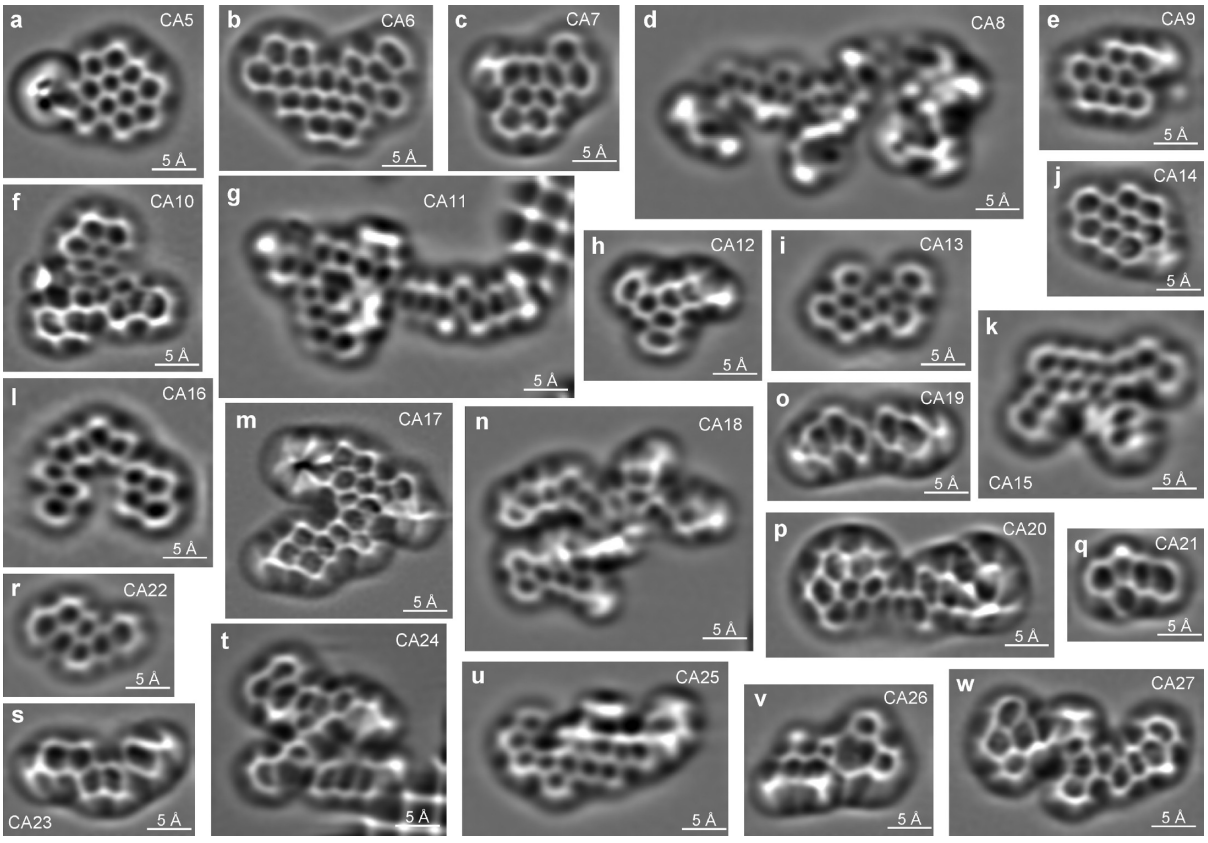

Figure 3. Coal-derived asphaltenes CA5-CA27. (a–w) Laplace-filtered AFM images of different CAs on Cu(111) or NaCl(2 ML)/Cu(111). In (g) and (t), a small patch of third-layer NaCl is also imaged. The AFM raw data and orbital images for some molecules are available in Figures S1 and S2, respectively.

RESULTS AND DISCUSSION

The combined use of AFM and STM for structure identification is demonstrated in Figure 1b–f. AFM is used to propose a hypothesis of the molecular structure, including some side groups. If molecular orbitals are accessible by STM, they can corroborate or refute the hypothesis. In Figure 1b–d, AFM measurements of the CA molecule **CA1** on NaCl(2 ML)/Cu(111) are shown. With decreasing tip height, the molecular structure that appears as repulsive (bright) contrast becomes more pronounced. This specific specimen has eight fused benzene rings with a small side-group attached at the topmost ring that we identified as CH_3 (see the Supporting Information). The rings appear distorted because the CO at the tip is tilting due to lateral forces.[23,36] From the STM orbital image shown in Figure 1f, we can learn about the electronic structure of **CA1**. The insulating NaCl layer decouples the molecule from the metallic substrate and allows us to tunnel into the substrate via the molecular orbital, if the latter lies in the applied bias window.[30] At the bias corresponding to the negative ion resonance (NIR), presented in Figure 1f, the STM topography resembles the lowest unoccupied molecular orbital (LUMO). This is confirmed by a density functional theory (DFT) calculation of the LUMO, using the structure hypothesis from AFM, as shown in Figure 1g.

The molecule **CA2** (Figure 2a–d) consists of eight fused benzene rings, subdivided into two aromatic parts: a pyrene and a methyl-substituted benzo[*c*]phenantrene moiety connected by a central five-membered ring. For this molecule, LUMO (Figure 2c) and the highest occupied molecular orbital (HOMO; Figure 2d) were accessible. They are in reasonable agreement with the calculated orbitals (see Figure S5), which are based on our structure hypothesis from AFM. In Figure 2e, an AFM image of **CA3** is shown. In regions where the contrast is weak, a Laplace-filtered image (Figure 2f) reveals additional details. The orbital images of the LUMO and HOMO (Figure 2g,h) were used to further elucidate the molecular structure (see Figure S6). Importantly, structural information mediated by orbital imaging is accessible in many cases where AFM cannot resolve the structure directly. **CA3** comprises other structural motifs, such as a fluorene moiety featuring a methylene bridge and a seven-membered ring.

In some cases (although in minor quantities), we also find CAs that have several (up to four) PAH islands connected by single covalent bonds. **CA4**, presented in Figure 2i–k, comprising two nonresonant PAHs, is such an example. Consequently, the LUMO (Figure 2k) is delocalized only over one side of the molecule. Another clear example of a molecule featuring two PAHs connected by a single bond is **CA16** in Figure 3l. This is a direct detection of the "archipelago"-type architecture reported in other publications.[13] However, in contrast to previous suggestions, we never observed PAHs that were connected by chains longer than a single bond.

Orbital imaging is in general an expedient complement to the atomic-resolution AFM images. It provides information about the delocalization of electrons in the frontier molecular orbitals, hence the degree of conjugation of the PAH core, and an independent cross-check for testing a structure hypothesis from AFM. The HOMO–LUMO gap, which is closely related to the difference between the NIR and the positive ion resonance

DOI: 10.1021/jacs.5b04056
J. Am. Chem. Soc. 2015, 137, 9870–9876

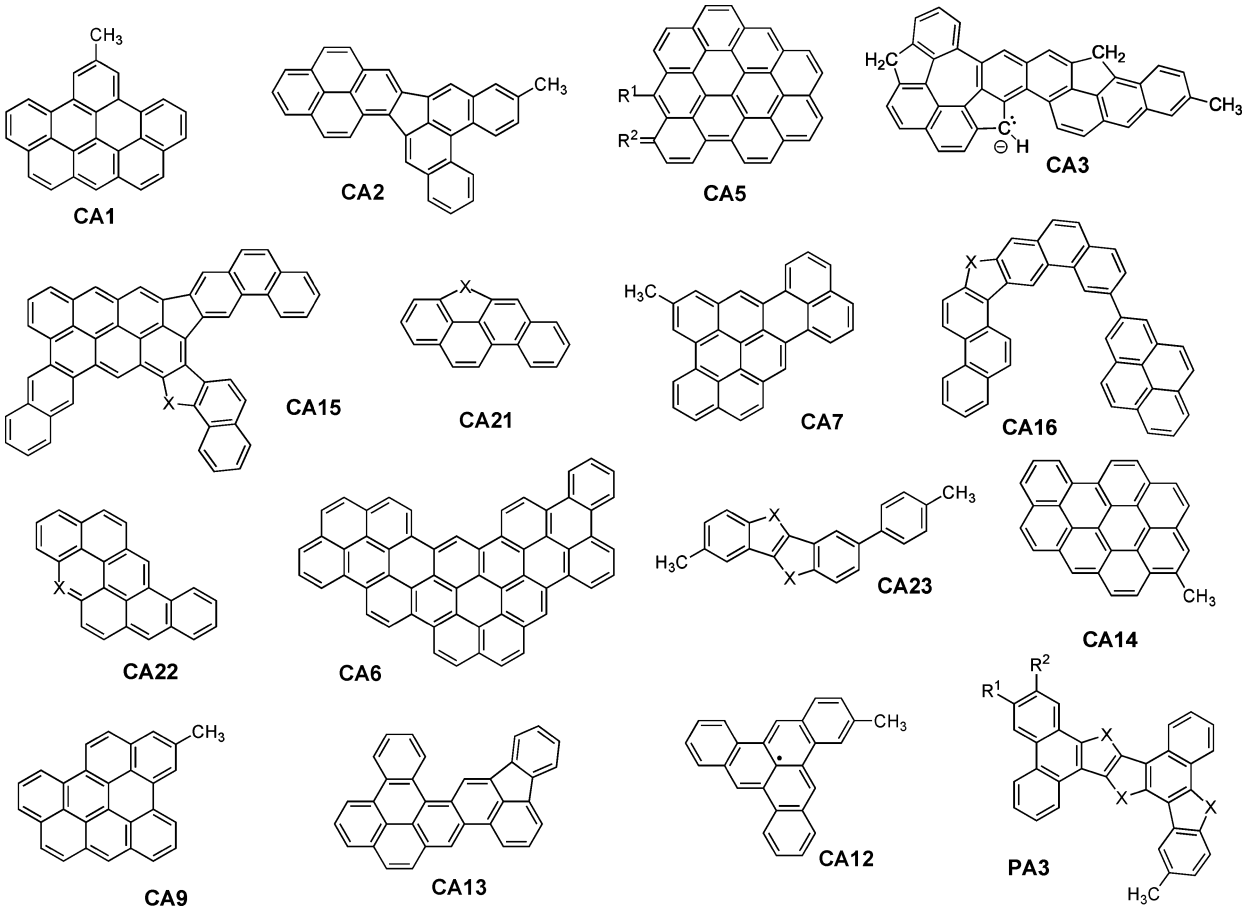

Figure 4. Proposed chemical structures. The proposed structures are based on AFM measurements and STM orbitals images. X denotes unknown moieties within the carbon framework (likely CH, CH_2, N, NH, Om or S), and R indicates unknown side groups.

(PIR) (NIR/PIR are related to the electron affinity and ionization energy of the molecule, respectively, by considering the polarizability of the substrate.[30]) that we can measure here, is also an indicator for the stability of the molecule.[37] This stability is expected to be exceptionally high for asphaltenes inferred from their long lifetimes on the order of geologic time scales.[38] Moreover, with orbital imaging, we can identify singly occupied orbitals[39] that indicate radicals (see Figures S2c and S7e–h). Finally, STM measurements of the resonance energies and geometries corresponding to the molecular orbitals can be employed for screening molecules for applications. For example for bipolar molecules in organic photovoltaic devices, besides staggered energy levels, it is important to have orbitals localized within different parts of the molecule[40−43] as observed for **CA4**.

In Figure 3 and Figures S1–S4, other atomic-resolution images of CAs are shown. The huge diversity of the different structures observed is formidable. In all of the about 100 atomic-resolution AFM measurements of CAs taken, we never observed two identical specimens. Typically, CAs have a single central PAH core containing about 4–20 rings, which are predominantly fused in a peri-condensed manner (e.g., Figure 3a), but also cata-condensed fragments can be observed (e.g., Figure 3g). The molecules tend to be slightly bigger than expected by considering mass limits and presuming one PAH per molecule.[3] Nevertheless, in most mass spectrometry (MS) studies of asphaltenes, an unidentified high-mass tail has been reported.[44] According to our measurements, we believe that these heavier molecules share the same molecular architectures as their lighter counterparts.

By analyzing each image in detail, one can identify additional interesting structural patterns, for example, a nine-membered macrocycle in Figure 3v, a molecule with four PAH islands in Figure 3t, and a molecule with exceptionally large side groups in Figure 3d, indicating incomplete cracking. Another remarkable specimen that was unambiguously identified is **CA6** (Figure 3b), a 18-ring nanographene. This suggests the exciting possibility of using asphaltenes to explore nanographenes with novel geometries.[45] In Figure 4 we present the proposed chemical structures for certain molecules that could be fully or partially identified.

CA molecules can be used to study PAHs of asphaltenes in general and are well suited for constant-height AFM imaging, because they are typically planar and have only a few side-chains. However, PAs are much more important from an economic standpoint and are known to have more and longer side-chains attached to the PAH core, which complicates both measurement and analysis. The PA investigated here is from virgin crude oil (which typically stems from aquatic organisms) and did not undergo additional physicochemical treatment (such as hydrogenation and cracking as CA). In Figure 5a,b AFM images of **PA1** are shown. This molecule has a large PAH core with two side-chains attached. We observe repulsive contrast on the side-chains already at a tip height that is 2 Å larger than the one needed to atomically resolve the PAH. This is indicative of the side-chains being less closely adsorbed on

DOI: 10.1021/jacs.5b04056
J. Am. Chem. Soc. 2015, 137, 9870−9876

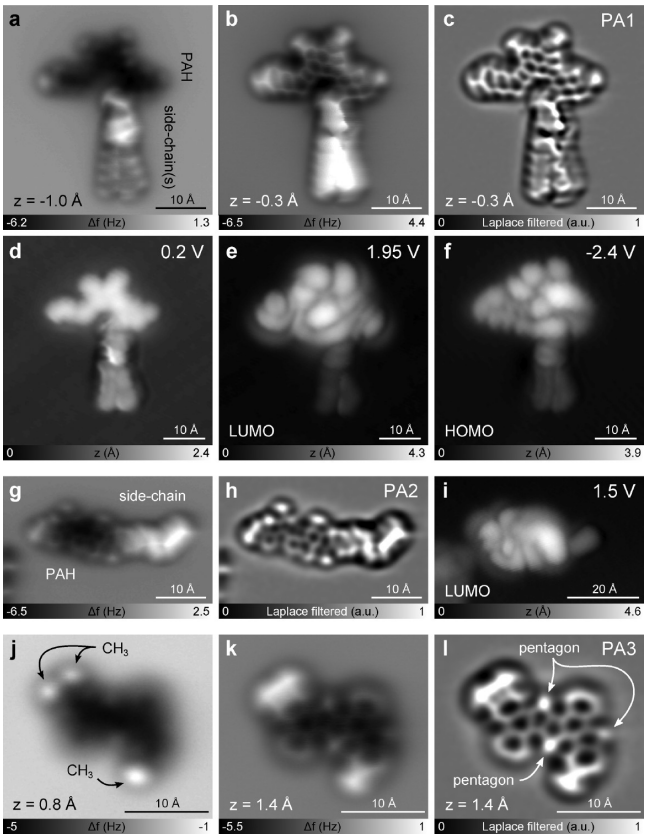

Figure 5. Petroleum asphaltenes PA1-PA3. (a,b) AFM images of **PA1** on NaCl(2 ML)/Cu(111) at different set-points z from (I = 1 pA, V = 0.2 V). (c) Laplace-filtered image of (b). (d–f) STM images (I = 1 pA) of **PA1** recorded at 0.2, 1.95, and −2.4 V, respectively. (g,h) AFM image of **PA2** on NaCl(2 ML)/Cu(111) (g) and its Laplace-filtered version (h). (i) STM orbital image (I = 0.6 pA) of **PA2** corresponding to the LUMO resonance. On the left side of (g–i) there is a small patch of third-layer NaCl. (j,k) AFM images of **PA3** on NaCl(2 ML)/Cu(111) at different set-points z from (I = 1.8 pA, V = 0.2 V). (l) Laplace-filtered image of (k).

the surface compared to the PAH.[46,47] The side-chains sometimes also undergo tip-induced conformational changes when being scanned in STM or AFM mode. As shown in Figure 5a, they often appear as zigzag-like patterns, associated with alkanes. In STM orbital images, these side-chains do not contribute (see Figure 5e,f). A similar example is **PA2** (Figure 5g–i), which has a side-chain of about 20 Å in length. Also here, the PAH core alone composes the orbital, which allows conclusions on its structure. Imaging orbitals are particularly important for PA as the peripheral alkanes can make interpretation of AFM images of PA difficult. Typically, PAs also exhibit more substituents and five-membered rings than CAs do. Exemplary, **PA3**, shown in Figure 5j–l, features three such pentagonal rings.

In summary, we find that asphaltene molecules consist of a central aromatic core with peripheral alkane chains. In some cases, this central core is divided into several distinct PAHs connected by a single bond, which proves the presence of "archipelago"-type molecules. Nevertheless, a single aromatic core with peripheral alkanes is the dominant asphaltene molecular architecture, proving the main aspects proposed by the Yen–Mullins model.[11] The diverse PAH architecture (number and type of rings and overall shape) of CAs and PAs is similar, despite significant differences in their formation and postprocessing. The main difference is the presence of longer side groups in PA. Additionally, PA contains more substituted rings. Both, CA and PA molecules are larger than expected from previous studies.[3,12,44]

The preparation procedure and single-molecule analysis presented here might raise doubts concerning the significance for the vast set of molecule structures in the mixture. In the following we address the main issues connected with the preparation and discuss the benefits and limitations related to our single-molecule approach. Thermally evaporating the molecules in UHV involves mainly two concerns: (i) sublimation of volatile, light components (about 100 u or less) in UHV at room temperature before evaporation onto the sample and (ii) dissociation of large molecules, which crack at temperatures lower than their sublimation temperature. The latter is expected to occur (in part) for molecules of about 1000 u or more.[27] Therefore, very large asphaltenes will not be detected, however, their relative abundance is known to be small[3,9,12,16,17,48,49] and visually we do not observe any residuals in the evaporator. Also for asphaltene samples we observe molecules with masses above 500 u on the surface, e.g., **CA6**, **CA11**, **CA17**, **CA18**, **PA1**, and **PA14** indicating that molecules of this size can be deposited without fragmentation. Non-covalently bonded globular aggregates that were shown to comprise a significant part of asphaltenes[2,15,49–51] are most likely disaggregated upon evaporation. Note that all molecules that are evaporated in the solid angle of the surface will be adsorbed because both the Cu and NaCl substrates have a sticking coefficient of unity at 10 K. On the surface we find almost exclusively individual molecules and no larger aggregates. The observation of no significant qualitative difference of the molecular structures on Cu and NaCl indicates that bond cleavage catalyzed by the Cu(111) surface is not an issue. However, the conformation of the molecules is influenced by the surface, as upon adsorption the molecules usually adopt a planarized conformation with respect to the gas phase. To study single molecules as opposed to an entire ensemble not only bears limitations but also unique benefits: Most importantly the existence of a specific molecule within a complex mixture can be provided even if the molecule is rare and the mixture divers, as it is the case in our study. On the downside, a universal quantification such as the mean molecular weight or the relative abundance is not feasible. These different advantages and challenges with respect to conventional techniques for structure elucidation as nuclear magnetic resonance, X-ray diffraction, and mass spectrometry render AFM a valuable complementary tool for the characterization of molecular mixtures.

■ CONCLUSIONS

This study shows that complex, polydisperse molecule mixtures can be analyzed by AFM and STM on a single-molecule basis with atomic-resolution. Understanding the chemistry and physics of asphaltenes, so important in many economic settings, requires proper characterization of the molecular architecture, and not just in terms of the mean molecular properties but also the range of molecular architectures found. Molecular imaging presented herein has resolved uncertainties about the mean molecular structures and also provided the first direct measurement of the tremendous range of molecular structures in asphaltenes.

More generally, this technique might be useful to study the traceability of a sample, that is, to characterize and identify the

DOI: 10.1021/jacs.5b04056
J. Am. Chem. Soc. 2015, 137, 9870–9876

origin of the raw material and chemical/physical processes involved in the formation of the compounds. Thus, methods that are typical for liquid phase biomarkers can now be brought into the realm of crude oil solids, the asphaltenes, by AFM and STM. Obviously, there is also a huge potential to analyze related carbon-based aromatic mixtures, such as vacuum residues, heavy fractions, tar, pitch, bitumen, etc. The demonstrated structure elucidation of mixtures by scanning probe microscopy constitutes a paradigm shift for the development of new molecules, e.g., for light emitting diodes and photovoltaic devices or molecular electronics: Many different molecules in a mixture can be screened by high-resolution scanning probe microscopy in a single preparation without going through a lengthy chemical synthesis, purification, and characterization for each one of them beforehand. Important properties of individual molecules, i.e., electron affinity level, ionization potential, shape, and extent of the molecular frontier orbitals are investigated by STM for hundreds of different molecules found in a mixture and their molecular structures are assigned *in situ* by AFM.

MATERIALS AND METHODS

STM/AFM Measurements. *Setup.* The experiments were performed using a home-built low-temperature ($T \approx 5$ K), ultrahigh vacuum ($p \approx 1 \times 10^{-10}$ mbar) combined STM and AFM. The sensor was based on a qPlus quartz-crystal cantilever design operated in the frequency-modulation mode (resonance frequency $f_0 \approx 30$ kHz, spring constant $k \approx 1800$ N/m, quality factor $Q \approx 14{,}000$, and oscillation amplitude $A \approx 0.5$ Å). The bias voltage was applied to the sample. STM images are taken in constant-current mode. AFM measurements were acquired in constant-height mode at $V = 0$ V. Positive height offsets z correspond to a distance decrease with respect to the STM set-point.

Sample Preparation. First, a Cu(111) single crystal was cleaned by repeated sputter (Ne^+) and anneal (900 K) cycles. Subsequently, NaCl was evaporated at about 270 K, such that (100)-oriented NaCl islands of mostly two atomic layers in thickness were formed. A low coverage (approximately 0.01 nm^{-2}) of CO was deposited on the surface ($T \approx$ 10 K) for tip preparation by admitting CO into the UHV chamber. The asphaltenes samples were prepared by spreading a small amount (a couple of grains) of the solid, dry material on a piece of Si wafer. Then, this Si wafer was flash-heated by resistive heating onto the cold sample.

Tip Preparation. For the microscope tip we used a 25 μm-thick PtIr wire, shortened and sharpened with a focused ion beam. Thereafter, we prepared a clean and sharp Cu tip by repeated indentations into the Cu surface. A functionalized CO tip was created by picking-up a single CO molecule from the surface.[22]

Structural Assignment. The assignment of the structures from the AFM images is based on previous works resolving molecules atomically by AFM with CO functionalized tips,[22−29,46,47] taking into account the known effect of distortions due to the tilting of the CO molecule at the tip.[23,36,52,53] For example, five- and six-membered rings are distinguished by the number of bond intersections and corners and by the respective positions and enclosed angles of adjacent moieties. Moreover, substitutional heteroatoms such as nitrogen, oxygen, or sulfur are usually revealed by their AFM contrast being different from that of carbon.[24,25,46] In addition, fully resolving the molecule is not required to assess the overall molecular topology.

Asphaltene Samples. *Coal-Derived Asphaltenes (CAs).* Coal-derived asphaltenes from Indonesia, Tanito Harum (TH), were studied.[9] The coals were liquefied and distilled, and the distillation residue was then extracted to obtain coal-derived asphaltenes. The typical liquefaction conditions were at a temperature of 450−465 °C, a pressure of 17 MPa (in part from added H_2), with a gas/feed slurry ratio of 0.7 N m^3 kg^{-1}, and a coal concentration in the feed slurry of 40 wt %. The distillation residue was the fraction boiling above 538 °C. The asphaltene fraction, which is toluene-soluble and *n*-hexane-insoluble, was obtained by Soxhlet extraction of the distillation residue.

Petroleum Asphaltenes (PAs). The petroleum asphaltene samples were prepared using 40 mL *n*-heptane added per gram of UG8 crude oil from Kuwait. After 24 h with occasional stirring, the resulting asphaltene precipitate was filtered and Soxhlet extracted with *n*-heptane until colorless.

ASSOCIATED CONTENT

Supporting Information

Complementary AFM and STM measurements of different coal-derived and petroleum asphaltenes, molecular orbital calculations, AFM measurements of a synthetic control compound, discussion about the representativeness of the measured molecules. The Supporting Information is available free of charge on the ACS Publications website at DOI: 10.1021/jacs.5b04056.

AUTHOR INFORMATION

Corresponding Authors

*bsc@zurich.ibm.com
*lgr@zurich.ibm.com

Notes

The authors declare no competing financial interest.

ACKNOWLEDGMENTS

We thank R. Allenspach for comments. We acknowledge financial support from the ERC Advanced Grant CEMAS (agreement no. 291194) and the EU project PAMS (610446). D.P. acknowledges the Spanish Ministry of Science and Competitiveness for financial support (MAT2013-46593-C6-6-P).

REFERENCES

(1) Gough, M.; Rowland, S. *Nature* **1990**, *344*, 648−650.
(2) Mullins, O. C.; Sheu, E. Y.; Hammami, A.; Marshall, A. G. *Asphaltenes, Heavy Oils, and Petroleomics*; Springer: New York, 2007; Vol. *1*.
(3) Groenzin, H.; Mullins, O. C. *J. Phys. Chem. A* **1999**, *103*, 11237−11245.
(4) Ancheyta, J.; Trejo, F.; Rana, M. S. *Asphaltenes: Chemical Transformation during Hydroprocessing of Heavy Oils*; CRC Press: Boca Raton, FL, 2010.
(5) Larter, S.; Bowler, B.; Li, M.; Chen, M.; Brincat, D.; Bennett, B.; Noke, K.; Donohoe, P.; Simmons, D.; Kohnen, M.; Allan, J.; Telnaes, N.; Horstad, I. *Nature* **1996**, *383*, 593−597.
(6) Head, I. M.; Jones, D. M.; Larter, S. R. *Nature* **2003**, *426*, 344−352.
(7) Aitken, C. M.; Jones, D.; Larter, S. *Nature* **2004**, *431*, 291−294.
(8) Sheng, J. *Modern Chemical Enhanced Oil Recovery: Theory and Practice*; Gulf Professional Publishing: Burlington, MA, 2010.
(9) Wargadalam, V. J.; Norinaga, K.; Iino, M. *Fuel* **2002**, *81*, 1403−1407.
(10) Bergmann, U.; Groenzin, H.; Mullins, O. C.; Glatzel, P.; Fetzer, J.; Cramer, S. *Chem. Phys. Lett.* **2003**, *369*, 184−191.
(11) Mullins, O. C. *Energy Fuels* **2010**, *24*, 2179−2207.
(12) Sabbah, H.; Morrow, A. L.; Pomerantz, A. E.; Zare, R. N. *Energy Fuels* **2011**, *25*, 1597−1604.
(13) Karimi, A.; Qian, K.; Olmstead, W. N.; Freund, H.; Yung, C.; Gray, M. R. *Energy Fuels* **2011**, *25*, 3581−3589.
(14) Alshareef, A. H.; Scherer, A.; Tan, X.; Azyat, K.; Stryker, J. M.; Tykwinski, R. R.; Gray, M. R. *Energy Fuels* **2011**, *25*, 2130−2136.
(15) McKenna, A. M.; Donald, L. J.; Fitzsimmons, J. E.; Juyal, P.; Spicer, V.; Standing, K. G.; Marshall, A. G.; Rodgers, R. P. *Energy Fuels* **2013**, *27*, 1246−1256.

DOI: 10.1021/jacs.5b04056
J. Am. Chem. Soc. 2015, 137, 9870−9876

(16) Borton, D.; Pinkston, D. S.; Hurt, M. R.; Tan, X.; Azyat, K.; Scherer, A.; Tykwinski, R.; Gray, M.; Qian, K.; Kenttämaa, H. I. *Energy Fuels* **2010**, *24*, 5548−5559.
(17) Tang, W.; Hurt, M. R.; Sheng, H.; Riedeman, J. S.; Borton, D. J.; Slater, P.; Kenttämaa, H. I. *Energy Fuels* **2015**, *29*, 1309−1314.
(18) Zuo, J. Y.; Mullins, O. C.; Freed, D.; Elshahawi, H.; Dong, C.; Seifert, D. J. *Energy Fuels* **2013**, *27*, 1722−1735.
(19) Mullins, O. C. Annu. *Annu. Rev. Anal. Chem.* **2011**, *4*, 393−418.
(20) Watson, B. A.; Barteau, M. A. *Ind. Eng. Chem. Res.* **1994**, *33*, 2358−2363.
(21) Zajac, G. W.; Sethi, N. K.; Joseph, J. T. *Scanning Microsc.* **1994**, *8*, 463−470.
(22) Gross, L.; Mohn, F.; Moll, N.; Liljeroth, P.; Meyer, G. *Science* **2009**, *325*, 1110−1114.
(23) Gross, L.; Mohn, F.; Moll, N.; Schuler, B.; Criado, A.; Guitián, E.; Peña, D.; Gourdon, A.; Meyer, G. *Science* **2012**, *337*, 1326−1329.
(24) Gross, L.; Mohn, F.; Moll, N.; Meyer, G.; Ebel, R.; Abdel-Mageed, W. M.; Jaspars, M. *Nat. Chem.* **2010**, *2*, 821−825.
(25) Hanssen, K. Ø; et al. *Angew. Chem., Int. Ed.* **2012**, *51*, 12238−12241.
(26) Van der Lit, J.; Boneschanscher, M. P.; Vanmaekelbergh, D.; Ijäs, M.; Uppstu, A.; Ervasti, M.; Harju, A.; Liljeroth, P.; Swart, I. *Nat. Commun.* **2013**, *4*, 2023.
(27) Schuler, B.; Collazos, S.; Gross, L.; Meyer, G.; Pérez, D.; Guitián, E.; Peña, D. *Angew. Chem., Int. Ed.* **2014**, *53*, 9004−9006.
(28) de Oteyza, D. G.; Gorman, P.; Chen, Y.-C.; Wickenburg, S.; Riss, A.; Mowbray, D. J.; Etkin, G.; Pedramrazi, Z.; Tsai, H.-Z.; Rubio, A.; Crommie, M. F.; Fischer, F. R. *Science* **2013**, *340*, 1434−1437.
(29) Riss, A.; Wickenburg, S.; Gorman, P.; Tan, L. Z.; Tsai, H.-Z.; de Oteyza, D. G.; Chen, Y.-C.; Bradley, A. J.; Ugeda, M. M.; Etkin, G.; Louie, S. G.; Fischer, F. R.; Crommie, M. F. *Nano Lett.* **2014**, *14*, 2251−2255.
(30) Repp, J.; Meyer, G.; Stojković, S.; Gourdon, A.; Joachim, C. *Phys. Rev. Lett.* **2005**, *94*, 026803.
(31) Gross, L.; Moll, N.; Mohn, F.; Curioni, A.; Meyer, G.; Hanke, F.; Persson, M. *Phys. Rev. Lett.* **2011**, *107*, 086101.
(32) Schulz, F.; Ijäs, M.; Drost, R.; Hämäläinen, S. K.; Harju, A.; Seitsonen, A. P.; Liljeroth, P. *Nat. Phys.* **2015**, *11*, 229−234.
(33) Aviram, A.; Ratner, M. A. *Chem. Phys. Lett.* **1974**, *29*, 277−283.
(34) Elbing, M.; Ochs, R.; Koentopp, M.; Fischer, M.; von Hänisch, C.; Weigend, F.; Evers, F.; Weber, H. B.; Mayor, M. *Proc. Natl. Acad. Sci. U. S. A.* **2005**, *102*, 8815−8820.
(35) Sariciftci, N.; Wudl, F.; Heeger, A.; Maggini, M.; Scorrano, G.; Prato, M.; Bourassa, J.; Ford, P. *Chem. Phys. Lett.* **1995**, *247*, 510−514.
(36) Weymouth, A. J.; Hofmann, T.; Giessibl, F. J. *Science* **2014**, *343*, 1120−1122.
(37) Ruiz-Morales, Y. *Asphaltenes, Heavy Oils, and Petroleomics*; Springer: New York, 2007; pp 95−137.
(38) Mango, F. D. *Nature* **1991**, *352*, 146−148.
(39) Repp, J.; Meyer, G.; Paavilainen, S.; Olsson, F. E.; Persson, M. *Science* **2006**, *312*, 1196−1199.
(40) Tang, C. W. *Appl. Phys. Lett.* **1986**, *48*, 183−185.
(41) Yu, G.; Gao, J.; Hummelen, J. C.; Wudl, F.; Heeger, A. J. *Science* **1995**, *270*, 1789−1790.
(42) Forrest, S. R. *MRS Bull.* **2005**, *30*, 28−32.
(43) Tao, C.; Sun, J.; Zhang, X.; Yamachika, R.; Wegner, D.; Bahri, Y.; Samsonidze, G.; Cohen, M. L.; Louie, S. G.; Tilley, T. D.; Segalman, R. A.; Crommie, M. F. *Nano Lett.* **2009**, *9*, 3963−3967.
(44) Pomerantz, A. E.; Hammond, M. R.; Morrow, A. L.; Mullins, O. C.; Zare, R. N. *J. Am. Chem. Soc.* **2008**, *130*, 7216−7217.
(45) Cai, J.; Ruffieux, P.; Jaafar, R.; Bieri, M.; Braun, T.; Blankenburg, S.; Muoth, M.; Seitsonen, A. P.; Saleh, M.; Feng, X.; Müllen, K.; Fasel, R. *Nature* **2010**, *466*, 470−473.
(46) Pavliček, N.; Fleury, B.; Neu, M.; Niedenführ, J.; Herranz-Lancho, C.; Ruben, M.; Repp, J. *Phys. Rev. Lett.* **2012**, *108*, 086101.
(47) Schuler, B.; Liu, W.; Tkatchenko, A.; Moll, N.; Meyer, G.; Mistry, A.; Fox, D.; Gross, L. *Phys. Rev. Lett.* **2013**, *111*, 106103.
(48) Mullins, O. C. *Asphaltenes, Heavy Oils, and Petroleomics*; Springer: New York, 2007; pp 1−16.
(49) Pomerantz, A. E.; Wu, Q.; Mullins, O. C.; Zare, R. N. *Energy Fuels* **2015**, *29*, 2833−2842.
(50) Andreatta, G.; Goncalves, C. C.; Buffin, G.; Bostrom, N.; Quintella, C. M.; Arteaga-Larios, F.; Pérez, E.; Mullins, O. C. *Energy Fuels* **2005**, *19*, 1282−1289.
(51) Hortal, A. R.; Hurtado, P.; Martínez-Haya, B.; Mullins, O. C. *Energy Fuels* **2007**, *21*, 2863−2868.
(52) Hapala, P.; Kichin, G.; Wagner, C.; Tautz, F. S.; Temirov, R.; Jelinek, P. *Phys. Rev. B: Condens. Matter Mater. Phys.* **2014**, *90*, 085421.
(53) Moll, N.; Schuler, B.; Kawai, S.; Xu, F.; Peng, L.; Orita, A.; Otera, J.; Curioni, A.; Neu, M.; Repp, J.; Meyer, G.; Gross, L. *Nano Lett.* **2014**, *14*, 6127−6131.

DOI: 10.1021/jacs.5b04056
J. Am. Chem. Soc. 2015, 137, 9870−9876